RSC Advances

PAPER

View Article Online
View Journal | View Issue

Cite this: *RSC Adv.*, 2016, **6**, 13110

Effect of the thermal treatment temperature of RuNi bimetallic nanocatalysts on their catalytic performance for benzene hydrogenation†

Lihua Zhu,*[ab] Jinbao Zheng,[b] Changlin Yu,[a] Nuowei Zhang,[b] Qing Shu,[a] Hua Zhou,[b] Yunhua Li[b] and Bing H. Chen*[b]

Received 18th November 2015
Accepted 5th January 2016

DOI: 10.1039/c5ra24424b

www.rsc.org/advances

The thermal treatment temperature of bimetallic nanocatalysts plays an important role in determining their catalytic performance. In this study, the synthesis of RuNi bimetallic nanoparticles (BNPs) supported on carbon black catalysts (denoted as RuNi BNSC) *via* hydrazine hydrate reduction and galvanic replacement reaction methods was reported. Then the effect of the annealing temperature in N_2 (uncalcined, 160, 230, 280, 380, 480, 580 and 680 °C) of RuNi BNSC on its catalytic activity for the benzene hydrogenation reaction was investigated. It was found that RuNi BNSC calcined at 380 °C exhibited outstanding catalytic activity in the liquid phase hydrogenation of benzene to cyclohexane, which was about 3–4 times higher than that of RuNi BNSC calcined at 680 °C, while RuNi BNSC annealed at 480 °C had no activity for this reaction. The characterization results of the catalysts indicated that various thermal treatment temperatures in N_2 affected the RuNi BNP size, chemical states of Ru and Ni, and RuNi bimetallic nanostructures and thus the catalytic properties.

1. Introduction

Bimetallic supported nanocatalysts are widely studied by researchers since they play a significant role in the field of chemical engineering, such as energy, environmental protection and food processing. Generally, the catalytic activity, selectivity and stability of the bimetallic nanocatalysts are highly dependent on their size,[1] shape,[2] composition,[3] and structure.[4–13] Therefore, the design and control of these features are particularly important for developing a catalyst with outstanding catalytic performance. Various simple methods such as the means of altering the thermal treatment conditions were adopted to control the size, chemical state and nanostructures of bimetallic nanoparticles and investigate the catalytic performance of the catalysts. For example, Wang *et al.*[14] prepared the Pt_3Co/C catalyst by the method of impregnation reduction. And the catalyst was annealed in $N_2 + H_2$ at different temperatures (400 °C and 700 °C), with Pt_3Co/C-400 and Pt_3Co/C-700 catalysts acquired. The bimetallic nanocatalysts were proved to be Pt_3Co/C-400–Pt_3Co alloy and Pt_3Co/C-700–Pt_3Co@Pt core–shell structure. The Pt_3Co@Pt exhibited higher activity and stability than Pt_3Co in the ORR reaction. Luo *et al.*[15] prepared $Au_{82}Pt_{18}$ NPs *via* molecular-capping-based colloidal synthesis method, loaded on carbon black. The as-obtained $Au_{82}Pt_{18}$/C catalyst was calcined in $N_2 + H_2$ at different temperatures (400 °C, 500 °C and >650 °C). The investigation revealed that when the annealing temperature at 400 °C or 500 °C, $Au_{82}Pt_{18}$ was mainly present in the form of Au–Pt alloy with relatively small particles, and the alloy properties of $Au_{82}Pt_{18}$-500 was better than $Au_{82}Pt_{18}$-400; but when the annealing temperature > 650 °C, $Au_{82}Pt_{18}$ mainly existed in the form of phase segregation, with relatively large particles. It was also found that $Au_{82}Pt_{18}$-500 was the most active in the electrocatalytic methanol oxidation reaction (MOR). According to above literatures, the structure, size and thus catalytic performance of bimetallic catalysts could be controlled by changing the thermal treatment temperature.

Currently, some works were related to the successful preparation of the RuNi BNPs with various nanostructures by the wet-chemical methods, such as Ni@Ru core–shell NPs,[16] Ru–Ni core–shell NPs[17,18] and RuNi alloy NPs.[19] And some of these bimetallic catalysts showed excellent catalytic activity for the dehydrogenation of ammonia borane. Additionally, based on the reported literatures, the Ni-based,[20,21] Pt-based,[22–28] Ru-based,[29–36] Rh-based[37] and bimetallic catalysts (Pd–Rh,[38] La–Ni,[39] Pt–Pd,[40] Rh–Ni[41] and Au–Pd[42]) are widely used in benzene hydrogenation to cyclohexane.

However, in this work, the RuNi bimetallic supported catalysts, with different size, chemical state and nanostructures

[a]*School of Metallurgy and Chemical Engineering, Jiangxi University of Science and Technology, Ganzhou 341000, Jiang Xi, China. E-mail: lihuazhu@stu.xmu.edu.cn; Fax: +86-592-2184822; Tel: +86-592-2185253*

[b]*Department of Chemical and Biochemical Engineering, National Engineering Laboratory for Green Productions of Alcohols–Ethers–Esters, College of Chemistry and Chemical Engineering, Xiamen University, Xiamen 361005, China. E-mail: chenbh@xmu.edu.cn*

† Electronic supplementary information (ESI) available. See DOI: 10.1039/c5ra24424b

(including RuO_2 nanoparticles-on-NiO nanoparticles and Ru@Ni core–thin shell) were obtained by modulating the thermal treatment temperature in N_2 and then characterized. And the Ru–Ni/NiO/C catalyst (Ru nanoclusters supported on Ni/NiO NPs) was prepared and characterized in our previous work.[43] The above three various nanostructural catalysts showed distinct catalytic properties in the reaction of benzene hydrogenation to cyclohexane. The intrinsic relationship between the annealing temperature thus the size, chemical state and nanostructure of RuNi BNPs and the catalytic activity of RuNi BNSC for benzene hydrogenation has been described in this study. Moreover, as the combination of Ni and Ru can significantly reduce the noble metal (Ru) content, it is also promising that such RuNi BNSC has potential to substitute the existing industrial catalysts for the hydrogenation of aromatics.

2. Experimental section

2.1 Chemicals

Carbon black (BLACK PEARLS 2000 LOT-1366221) was purchased from Cabot Corporation and used as support. Nickel(II) chloride hexahydrate ($NiCl_2 \cdot 6H_2O$), anhydrous ethanol, NaOH, anhydrous $RuCl_3$, polyvinyl pyrrolidone (PVP), 85 wt% (weight percent) hydrazine hydrate solution and other reagents were purchased from Sinopharm Chemical Reagent Co. Ltd. (Shanghai, China). The deionized water produced by Milli-Q Intergral 3 (Millipore Corporation) was used in all the experiments. All reagents were used as received.

2.2 Catalysts preparation

$Ni/Ni(OH)_2/C$ was synthesized by hydrazine hydrate reduction method.[43–46] The brief steps are described as follows: 0.300 g of PVP and 12.5 mL of anhydrous ethanol were added in sequence into 82.5 mL of aqueous nickel(II) chloride hexahydrate ($NiCl_2 \cdot 6H_2O$ = 0.225 g) solution, magnetic stirring at RT for ten minutes. Then 12.5 mL of aqueous NaOH solution containing 1.813 g of NaOH was injected into the above solution. After ten minutes, 25 mL of 85 wt% hydrazine hydrate solution was added into the as-obtained liquid. Subsequently, ten minutes later, the addition of 1.250 g of carbon black was carried out. The whole synthesis process was under vigorous agitation at RT in a Teflon cup for 18 hours. Then the solids were collected by filtration, thoroughly washed with deionized water and anhydrous ethanol. $Ni/Ni(OH)_2/C$ was obtained after dried in a vacuum oven at 60 °C for 6 h, denoted as $Ni/Ni(OH)_2/C$–PVP. Another type of $Ni/Ni(OH)_2/C$ was also prepared by the same method, only without adding PVP during the process, signed as $Ni/Ni(OH)_2/C$. The total Ni loading including Ni element in $Ni(OH)_2$ was 2.48 wt%. All the $RuNi/Ni(OH)_2/C$ catalysts were obtained *via* galvanic displacement method,[47–51] *i.e.* adding an aqueous solution of $RuCl_3$ (9.64×10^{-3} mol L^{-1}) into the $Ni/Ni(OH)_2/C$ samples. Then Ru atoms were anchored onto $Ni/Ni(OH)_2$ NPs and supported on carbon black. Two different series of the RuNi/C catalysts were obtained by the above described galvanic replacement reaction, the first type of catalyst; signed as RuNi/C-uncalcined–PVP with loadings of Ru 1.25 wt% and Ni 1.40 wt%, respectively; the second type of catalyst, signed as RuNi/C-uncalcined (without using PVP) with loadings of Ru 1.25 wt% and Ni 1.40 wt%, respectively. Then all these uncalcined RuNi bimetallic catalysts were annealed in flowing 99.999% N_2 (80 mL min^{-1}) at specific set temperature for 3 h with the heating rate of 2 °C min^{-1}, denoted as RuNi/C-*X*–PVP and RuNi/C-*X*, respectively, where *X* = (uncalcined, 160, 230, 280, 380, 480, 580 and 680) respectively is the annealing temperature. The Ru and Ni loading in the other RuNi/C-*X*–PVP and RuNi/C-*X* catalysts is approximately equal to 1.40 wt% and 1.25 wt% determined by ICP-MS technique, respectively. And the RuNi/C-380–PVP catalyst was synthesized by us in the prior period.[43] The Ni and Ru loadings for all samples were quantitatively determined and confirmed by ICP-MS technique (Agilent ICP-MS 4500-300) resulting in Ni and Ru content in RuNi/C-380 1.398 wt% and 1.246 wt%, respectively.

$Ni/NiO/C$ can be gained as $Ni/Ni(OH)_2/C$–PVP calcined in N_2 at 380 °C for 3 h. The Ru/C catalysts with Ru loading of 1.25 wt% or 2.5 wt% were prepared by incipient wetness impregnation and then reduced in flowing N_2 + 10% H_2 (80 mL min^{-1}) at 380 °C or 600 °C for 3 h, denoted as 1.25% Ru/C-380–N_2 + H_2 and 2.5% Ru/C-600–N_2 + H_2, respectively. Carbon-380 was obtained after carbon black annealed in N_2 at 380 °C for 3 h.

2.3 Catalyst characterization

XRD analysis for the samples was performed on a Rigaku Ultima IV X-ray diffractometer equipped with high-speed array detection system and CuKα radiation (35 kV and 20 mA) as the X-ray source. Scans were performed over the 2θ range of 10–90° with a scanning rate of 10° min^{-1}.

X-ray photoelectron spectroscopy (XPS) measurements for the samples were performed on PHI Quantum 2000 Scanning ESCA Microprobe equipment with monochromatic AlKα radiation. Transmission electron microscope (TEM) and high resolution transmission electron microscope (HRTEM) images for the catalysts were conducted on a FEI TECNAI F30-HRTEM with a field emission source and the accelerating voltage is 300 kV. The high-angle annular dark field scanning transmission electron microscopy (HAADF-STEM), STEM-EDS mapping and line-scan analysis for the RuNi/C-680–PVP sample was performed on FEI TECNAI F20-HRTEM operated at 200 kV. Prior to the tests, the catalysts were dispersed onto a copper grid coated with a thin holey carbon film.

High-sensitivity low-energy ion scattering (HS-LEIS) test was performed on an IonTOF Qtac100 low-energy ion scattering analyzer, with a $^{20}Ne^+$ beam energy of 5 keV with a sample current 1.6 nA and a low ion flux equal to 445 pA cm^{-2} and the scattering angle was 145°.

2.4 Catalytic performance measurement

The catalytic behavior of the catalysts for benzene hydrogenation to cyclohexane was examined in a stainless steel high pressure reactor (Parr 4848). In a typical experiment, 10 mL of benzene and 50 mg of catalyst were introduced into the autoclave and then the reactor was purged with 99.999% N_2 for 1 min and with 99.999% H_2 for another 1 min. Hydrogen was

introduced to the container up to 4.8 MPa, under a constant stirring rate of 500 rpm, the mixture was then programmed to the required temperature (60 °C) and the reaction pressure reached 5.3 MPa and the reaction was performed for 1 h. When the reaction reached the set time, the reactor was cooled to 5 °C using an ice-water bath. And the gas within the reactor was liberated after cooling. The reaction mixture was analyzed by gas chromatography (GC) on a Shimadzu GC 2010 equipped with a DB-35 60 m × 0.32 mm capillary column and a flame ionization detector (FID), and gas chromatography-mass spectrometry (GC-MS) on a Shimadzu GC-MS 2010. The TOF (turnover frequency) of the catalyst was calculated based on the moles of total Ru metal. There are two main reasons for not taking the metal dispersion into account in the calculation of TOF: firstly, the metal dispersion was not provided for most of the supported catalysts for the liquid benzene hydrogenation in the literatures (as shown in Table S1†), for comparison, the Ru metal dispersion was not measured in this work; secondly, Ni element mainly in the form of NiO in the catalysts.

3. Results and discussion

3.1 The catalytic performance of the catalysts

The catalytic activity of as-synthesized catalysts was evaluated using benzene hydrogenation to cyclohexane under relatively mild conditions: reaction pressure, 5.3 MPa H_2; reaction temperature, 60 °C; reaction time, 1 h. The catalytic reaction results of different as-prepared catalysts are listed in Tables 1 and 2. From the results shown in tables, there was no any product when using carbon black as the catalyst (Table 1, entry 1). Small amount of cyclohexane with the yield below 0.1% (Table 1, entry 2) was obtained over the Ni/NiO/C catalyst. When the reaction was performed over 1.25% Ru/C-380–N_2 + H_2 (380 represents the annealing temperature in N_2 + H_2 and 1.25% is the Ru loading), the yield toward cyclohexane was 9.42%, with TOF of 1706.0 h^{-1} (Table 1, entry 3). For the RuNi/C-*X*–PVP catalysts, when the calcination temperature of the catalyst lower than or equal to 280 °C, the yield to cyclohexane was very low (entries 4–7 in Table 1). However, the RuNi/C-380–PVP catalyst (Ru–Ni/NiO/C) exhibited a 100% yield to cyclohexane and high catalytic activity (18 210.3 h^{-1}) (entry 8 in Table 1).[43] It could come with two main reasons. Firstly, PVP remained in the catalyst when annealed at low temperature (≤280 °C), and it hindered the adsorption and diffusion of reactants. As the annealing temperature increasing to 380 °C, PVP would be discomposed and $Ni(OH)_2$ was simultaneously decomposed into NiO and H_2O.[43] Secondly, it is generally accepted that low thermal treatment temperature could lead to the RuNi BNPs becoming smaller, and too small RuNi BNPs were perhaps unfavorable to activate benzene molecular.[52,53] More surprisingly, if the calcination temperature rose to 480 °C, the catalyst did not have any activity (Table 1, entry 9). But benzene hydrogenation was successfully carried out over the RuNi/C-580–PVP and RuNi/C-680–PVP catalysts, with the TOF of 2993.8 and 5299.2 h^{-1}, and the yields to cyclohexane of 16.44% and 29.10% (entries 10, 11 in Table 1), respectively. The above results imply that the thermal treatment temperature of the catalysts could greatly influence their catalytic properties. The intrinsic nature of the effect of thermal treatment temperature on catalytic performance would be examined and stated in the section of characterizations.

Table 1 Catalytic performance of the RuNi/C-*X*–PVP catalysts under different calcination temperatures in N_2 for benzene hydrogenation to cyclohexane[a]

Entry	Catalyst (0.05 g)	TOF[b] (h^{-1}) × 10^3	Yield to cyclohexane
1	Carbon	—	No product
2	Ni/NiO/C	—	<0.1%
3	1.25% Ru/C-380–N_2 + H_2	1.70	9.42%
4	RuNi/C-uncalcined–PVP	0.03	0.14%
5	RuNi/C-160–PVP	0.19	1.05%
6	RuNi/C-230–PVP	0.47	2.60%
7	RuNi/C-280–PVP	0.60	3.30%
8	RuNi/C-380–PVP	18.21	100% (ref. 43)
9	RuNi/C-480–PVP	0.10	0.53%
10	RuNi/C-580–PVP	2.99	16.44%
11	RuNi/C-680–PVP	5.30	29.10%

[a] All entries were conducted under the following reaction conditions: reaction pressure, 5.3 MPa H_2; reaction temperature, 60 °C; reaction time, 1 h; benzene, 10 mL. [b] The TOF (turnover frequency) of the catalysts was calculated as: conversion of moles of benzene per mole of ruthenium per hour.

To further confirm the effect of PVP on the catalytic activity for benzene hydrogenation, the RuNi/C-*X* catalysts with the same Ru and Ni loading as RuNi/C-*X*–PVP (without the addition of PVP during the catalyst synthesis process) were also prepared. The RuNi/C-*X* catalysts were annealed in flowing N_2 (80 mL min^{-1}) at various temperatures for 3 h. They were also evaluated by the reaction of benzene hydrogenation to cyclohexane and the results are listed in Table 2. With the annealing temperature increasing from uncalcined to 380 °C, the conversion of benzene gradually grew from 1.47% to 42.5% (entries 1–5, Table 2). Whereas, the thermal treatment temperature reached at 480 °C (RuNi/C-480), no cyclohexane produced (entry

Table 2 Catalytic performance of the RuNi/C-*X* catalysts (meaning without the addition of PVP) under different calcination temperatures in N_2 for benzene hydrogenation to cyclohexane[a]

Entry	Catalyst (0.05 g)	TOF[b] (h^{-1}) × 10^3	Yield to cyclohexane
1	RuNi/C-uncalcined	0.27	1.47%
2	RuNi/C-160	0.33	1.83%
3	RuNi/C-230	1.69	9.25%
4	RuNi/C-280	5.62	30.85%
5	RuNi/C-380	7.75	42.5%
6	RuNi/C-480	0.05	0.20%
7	RuNi/C-580	2.17	11.9%
8	RuNi/C-680	4.60	25.2%

[a] All entries were conducted under the following reaction conditions: reaction pressure, 5.3 MPa H_2; reaction temperature, 60 °C; reaction time, 1 h; benzene, 10 mL. [b] The TOF (turnover frequency) of the catalysts was calculated as: conversion of moles of benzene per mole of ruthenium per hour.

6 Table 2). But RuNi/C-580 and RuNi/C-680 provided a TOF of 2172.8 h^{-1} and a 11.9% yield to cyclohexane (entry 7, Table 2), a TOF of 4601.2 h^{-1} and a 25.2% yield to cyclohexane (entry 8, Table 2), respectively. It shows that the relationship between the calcination temperature and catalytic properties for the RuNi/C-*X* catalysts is quite consistent with that for the RuNi/C-*X*–PVP catalysts in the thermal treatment temperature range. Compared the activity of RuNi/C-280–PVP (TOF-600.9 h^{-1} and yield-3.30%) (entry 7 in Table 1) with that of RuNi/C-280 (TOF-5621.1 h^{-1} and yield-30.85%) (entry 4 in Table 2), it demonstrates that undecomposed PVP could hinder reactants diffusing to active sites and slow down the reaction rate. Moreover, the RuNi/C-380 catalyst exhibited relatively high catalytic performance in benzene hydrogenation reaction compared to a number of supported or unsupported Ru-based, Rh-based, Pd-based, Ir-based and bimetallic-based catalysts reported in literatures (Table S1†). The high catalytic activity of the RuNi/C-380 catalyst is mainly due to the nanostructure of Ru nanoclusters supported on Ni/NiO nanoparticles thus the synergy effect of multiple active sites (Ru, Ni and NiO sites), suitable size of RuNi bimetallic nanoparticles, and chemical states of Ni or Ru element. These details will be characterized below. Additionally, the Ru–Ni bimetallic nanocatalysts showed the high stability in aromatic hydrogenation reactions in our previous works.[44,45]

Fig. 1 shows the comparison of the catalytic performance of the above two series of the catalysts. It was found that the thermal treatment temperature of the RuNi/C catalysts played an important role in determining their catalytic activity. This is because the annealing temperature strongly affects the decomposition of PVP, size and nanostructure of RuNi BNPs and chemical states of Ni and Ru. These conclusions will be fully proved by an array of characterizations, as described in the following subsections.

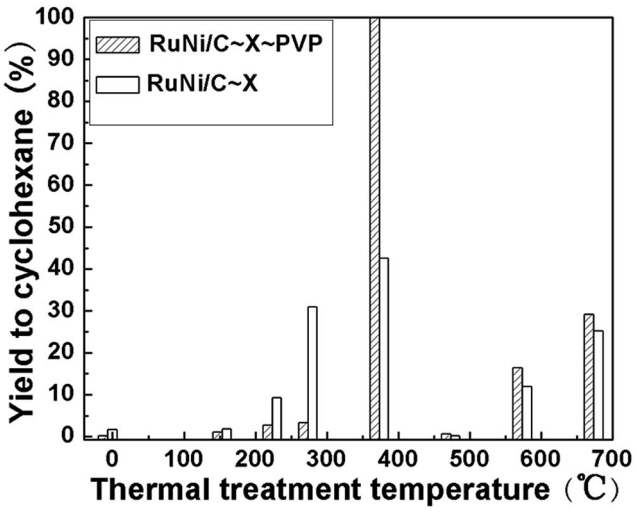

Fig. 1 Comparisons of the catalytic performance of the RuNi/C-*X*–PVP and RuNi/C-*X* catalysts for the hydrogenation of benzene to cyclohexane.

3.2 XRD patterns for the catalysts

To discover the links of the distinct catalytic performance of the RuNi/C-*X* (or RuNi/C-*X*–PVP) catalysts to the nanostructures of RuNi BNPs as well as the Ru or Ni chemical state in the RuNi/C-*X* catalysts, firstly, powder X-ray diffraction (XRD) for carbon-380, 2.5% Ru/C-600–N_2 + H_2 and RuNi/C-*X* samples were performed. As shown in Fig. 2, two diffraction peaks are clearly observed for carbon, attributed to carbon (002) and carbon (100).[54–56] All the diffraction peaks for Ru/C are characteristic of hexagonal close packed (hcp) Ru, corresponding to planes (100) ($2\theta = 38.6°$), (002) ($2\theta = 42.3°$), (101) ($2\theta = 44.1°$), (102) ($2\theta = 58.6°$), (110) ($2\theta = 70.0°$) and (103) ($2\theta = 79.3°$) (JCPDS card no. 06-0663). Only diffraction peaks of carbon (002) and carbon (100)[54–56] (or NiO (200) ($2\theta = 43.3°$) (JCPDS card no. 47-1049)) can be seen for the RuNi/C-380 sample, no any other diffraction peak for Ru, indicating that Ru NPs either very small or amorphous. On the other hand, when the calcination temperature increased to 480 °C, the diffraction peaks of RuO_2 (101) ($2\theta = 35.0°$), RuO_2 (211) ($2\theta = 54.3°$) (JCPDS card no. 43-1027) and NiO (200) ($2\theta = 43.3°$) (JCPDS card no. 47-1049) appeared, suggesting the presence of Ru oxidation state (RuO_2) and NPs size becoming larger. However, based on the temperature programmed reduction (TPR) results in our previous works,[48] RuO_2

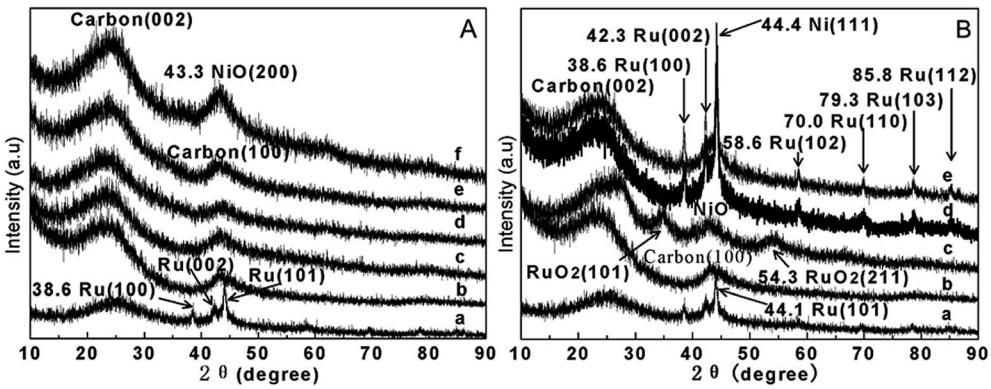

Fig. 2 Powder X-ray diffraction (XRD) patterns for the RuNi/C-*X* samples. (A) (a) 2.5% Ru/C-600–N_2 + H_2, (b) carbon-380, (c) RuNi/C-uncalcined, (d) RuNi/C-160, (e) RuNi/C-280 and (f) RuNi/C-380. (B) (a) 2.5% Ru/C-600–N_2 + H_2, (b) carbon-380, (c) RuNi/C-480, (d) RuNi/C-580 and (e) RuNi/C-680.

$$2NiO+C\rightarrow 2Ni+CO_2;\quad RuO_2+C\rightarrow Ru+CO_2$$

Scheme 1 The chemical equation for the process of NiO and RuO_2 reduced by carbon at high temperature.

in the body phase can only be reduced at ~120 °C, much higher than the reaction temperature in this work (60 °C). So it can be considered that Ru in RuNi/C-480 mainly existed in the form of RuO_2 in the reaction. To some extent, the variations of Ru chemical states and RuNi BNPs size obtained in the XRD patterns reflect the difference in catalytic performance of the RuNi/C-380 and RuNi/C-480 catalysts, since RuO_2 has weak capability to activate and dissociate hydrogen molecular (H_2) at relatively low temperature (60 °C). With the increase of the calcination temperature to 580 °C or 680 °C, according to Scheme 1, NiO and RuO_2 were reduced by carbon due to its reducing capacity.[57] In this case, the Ni (111) diffraction peak was clearly seen, and other peaks at $2\theta = 38.6°$, 42.3°, 44.1°, 58.6°, 70.0°, 79.3° and 85.8° can be indexed with Ru (100), (002), (101), (102), (110), (103) and (112), respectively (JCPDS card no. 06-0663). From these XRD results, we may find the reasons that the RuNi/C-580 and RuNi/C-680 catalysts exhibited higher catalytic performance than the RuNi/C-480 catalyst. But the activity of these two catalysts is still much lower than the RuNi/C-380 catalyst owing to the absence of the multiple and synergetic active sites (Ru, Ni and NiO).[43] Additionally, based on the XRD characterizations, the diffraction peaks in the patterns for the RuNi/C-*X* catalysts are without any shift, compared to the Ru/C and Ni/C catalysts. It indicates that Ru and Ni in the RuNi BNPs are in phase segregation not in RuNi alloy for the RuNi bimetallic catalysts annealed in N_2.

The XRD tests for the RuNi/C-*X*–PVP catalysts were also carried out. As depicted in Fig. S1,† the interpretations for them are given in ESI.† Similar conclusions can be obtained. But no any diffraction peak due to Ru or Ni species is present for the RuNi/C-380–PVP sample (Fig. S1c†). Additionally, the intensity of each diffraction peak in the XRD patterns for the RuNi/C-*X* samples is much stronger and sharper than that of the corresponding diffraction peak in the XRD patterns for the RuNi/C-*X*–PVP samples (Fig. 2 and S1†). It implies that PVP played a vital role as dispersing and protecting agent, resulting in better dispersion and smaller size of RuNi BNPs in the RuNi/C-380–PVP catalyst. Therefore, the RuNi/C-380–PVP catalyst was about 2 times more active than the RuNi/C-380 catalyst for the hydrogenation of benzene to cyclohexane under the same reaction conditions.

Based on the above XRD patterns and catalytic activity of the catalysts in benzene hydrogenation, it could be found that RuO_2 has nearly no capacity of activating hydrogen molecular thus led to low catalytic activity in benzene hydrogenation reaction, while Ru(0) has.

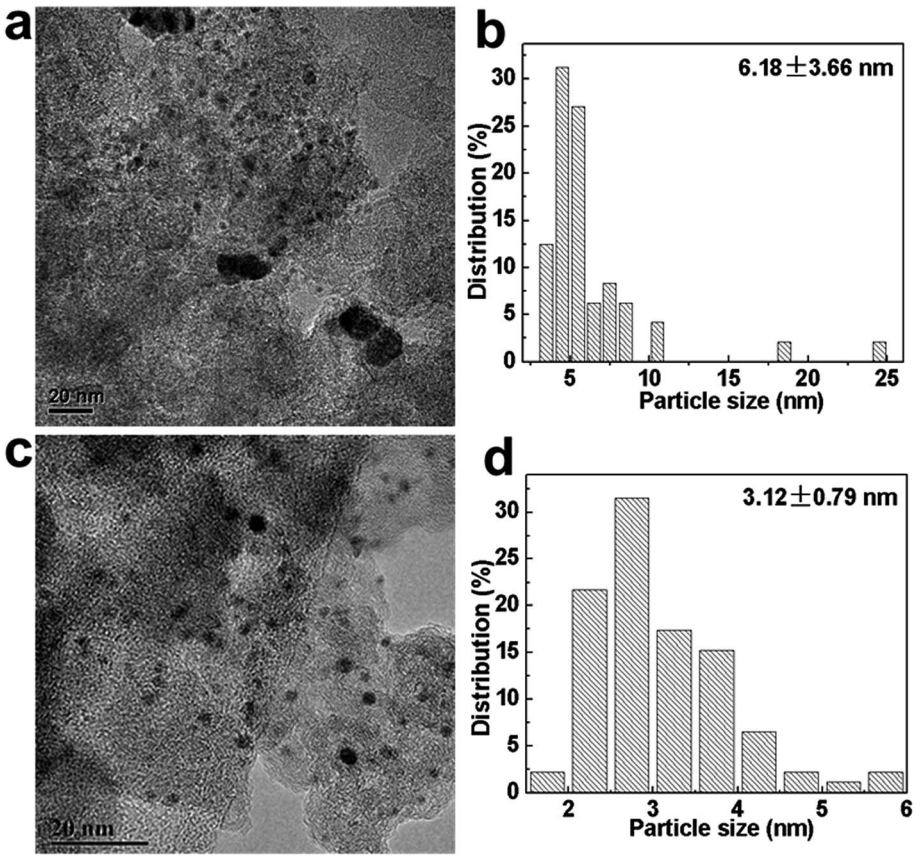

Fig. 3 TEM image and RuNi NPs size distribution for (a and b) RuNi/C-480–PVP and (c and d) RuNi/C-680–PVP. Scale bar, 20 nm.

3.3 XPS analysis of the catalysts

X-ray photoelectron spectroscopy (XPS) tests were carried out to obtain the chemical states of Ru and Ni in the RuNi/C-*X*–PVP samples. As shown in Fig. S2A,† it indicates that the main Ni-species on the surface of the RuNi/C-*X*–PVP catalysts (X = 380, 480 or 680) is Ni oxidation state (NiO, $Ni(OH)_2$ and NiOOH).[58–60]

Ru 3p XPS spectra for the catalysts are shown in Fig. S2B.† For the RuNi/C-380–PVP sample, it implies the co-existence of Ru(0) and RuO_2.[61–63] The formation of RuO_2 is resulted from the surface oxidation of Ru(0) NPs exposed in air prior to test.[33] While the main Ru-species is RuO_2 in the RuNi/C-480–PVP catalyst. On the contrary, Ru element mainly in the form of Ru(0) is present in the RuNi/C-680–PVP sample. So it is very likely that Ru@Ni core–shell nanostructure has formed in RuNi/C-680–PVP, and Ni shell layer might protect Ru core against surface oxidation.

The XPS results are considerably consistent with the above XRD patterns for the samples. Associating with the catalytic activity and XPS tests results, the synergetic effect of Ru(0), Ni(0) and NiO is very favorable for enhancing the catalytic property in benzene hydrogenation to cyclohexane, but the excessive existence of RuO_2 is disadvantageous for the reaction.

Because the Ru and Ni loading in the RuNi/C-*X*–PVP samples are relatively low, RuNi BNPs are so small or amorphous and well dispersed, the XPS signals for Ru and Ni are too weak. Therefore, to further confirm the above conclusions, the HRTEM, HAADF-STEM, EDS-elemental mapping and HS-LEIS tests should be performed for these samples, as described below.

3.4 TEM and HRTEM characterization of the samples

The representative transmission electron microscopy (TEM) and high resolution transmission electron microscope (HRTEM) images for the Ni/NiO/C and Ru/C catalysts are present in Fig. S3 and S4.† The HRTEM image for Ni/NiO/C displays the lattice fringes with interplanar spacing of 0.202 nm and 0.243 nm, corresponding to (111) planes of face-centered cubic (fcc) Ni (JCPDS card no. 04-0850) and (111) planes of fcc NiO (JCPDS card no. 47-1049), respectively. The HRTEM image for 1.25% Ru/C-380–N_2 + H_2 shows the lattice fringes with a regular spacing of 0.206 nm, due to Ru (101) planes (JCPDS card no. 06-0663). The metallic NPs could not be observed at all in as-obtained images for the RuNi/C-uncalcined–PVP sample (Fig. S5†). This is probably because NPs are too small (<1 nm) to be seen. In addition, the average size of RuNi BNPs (1.82 nm) in the RuNi/C-160 sample was much smaller than that of RuNi BNPs in RuNi/C-380 or RuNi/C-380–PVP (3.51 nm (ref. 43)) (Fig. 2 and S1, S6 and S7†). Too small RuNi BNPs are maybe unfavorable for the activation of benzene molecular.[52,53] It was the primary reason for the low catalytic activity of the RuNi/C-*X* catalysts treated at below or equal to 280 °C.

TEM images for the RuNi/C-*X*–PVP samples (X = 480 or 680) and RuNi NPs size distribution for these three catalysts are given in Fig. 3. The RuNi NPs mean size for these three catalysts were 6.18 nm (in the range of 1–25 nm) and 3.12 nm (1–6 nm), respectively. The RuNi NPs size distributions for the RuNi/C-380–PVP (1–8 nm (ref. 43)) and RuNi/C-680–PVP catalysts were relatively narrow, but that of RuNi/C-480–PVP was wider except for larger RuNi NPs. This is regarded as the secondary reason for RuNi/C-480–PVP less active in the reaction of benzene hydrogenation to cyclohexane.

Fig. 4 provides the HRTEM images for the RuNi/C-*X*–PVP samples (X = 380, 480 or 680). After RuNi/C-uncalcined–PVP was calcined in N_2 at 380 °C for 3 h. The HRTEM images (Fig. 4a and b) clearly display lattice fringes with a regular spacing of 0.240 nm, which could be attributed to the (111) facets of fcc NiO (JCPDS card no. 47-1049). The HRTEM image for the same RuNi BNP also shows lattice fringes with a distance of 0.214 nm on the surface of RuNi BNP (Fig. 4b), assigned to the (002) facets of hcp Ru (JCPDS card no. 06-0663), which implies that Ru was loaded on the NiO surface. Additionally, for most of the RuNi BNPs in RuNi/C-380–PVP, only lattice fringes of NiO can be observed. It indicates that Ni element was mainly in the form of

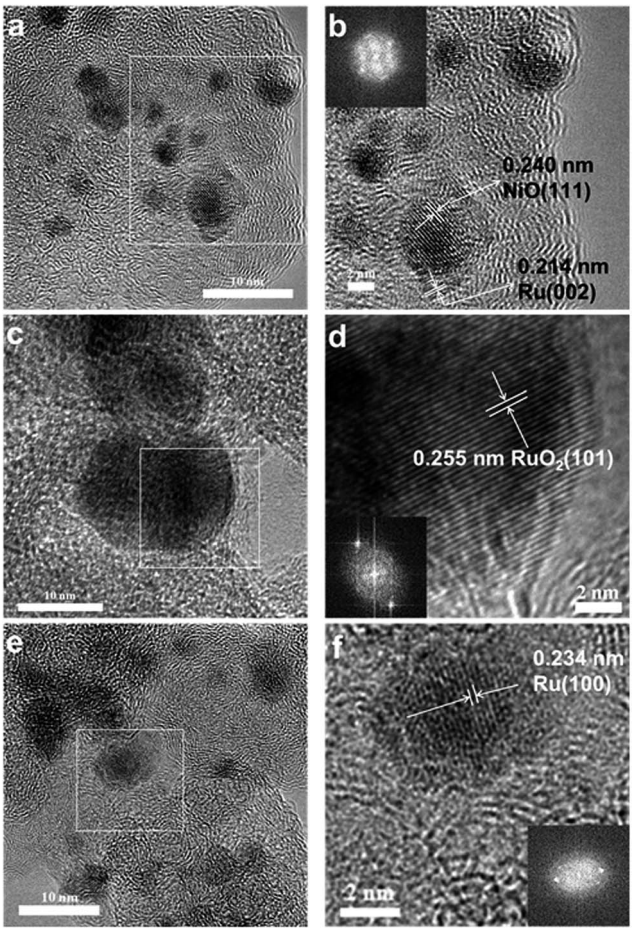

Fig. 4 HRTEM images for the RuNi/C-*X*–PVP catalysts. (a) RuNi/C-380–PVP. Scale bar, 10 nm. (b) Enlarged view of the selected area in image (a). Scale bar, 2 nm. (c) RuNi/C-480–PVP. Scale bar, 10 nm. (d) Enlarged view of the selected area in image (c). Scale bar, 2 nm. (e) RuNi/C-680–PVP. Scale bar, 10 nm. (f) Enlarged view of the selected area in image (e). Scale bar, 2 nm. Where the insets show their respective fast Fourier transform (FFT) patterns results.

NiO and Ru in the form of isolated and tiny nanoclusters supported on the Ni/NiO NPs in RuNi/C-380–PVP, which is in good accord with our previous reported results.[43] The structure of Ru nanoclusters-on-Ni/NiO nanoparticles is quite advantageous to increase catalytic performance in benzene hydrogenation to cyclohexane, owing to synergetic effect (specialization and cooperation) of Ru (activating H_2), NiO (activating benzene) "*via* interaction of its pi-electrons with the positively-charged sites of nickel oxide (P-type semiconductor with holes)"[64] and Ni sites (as a "bridge" for transferring activated H species to the activated benzene).[43,65–69] The X-ray absorption near edge structure (XANES) and extended X-ray absorption fine structure (EXAFS) spectra for the Ru–Ni/NiO/C catalyst in hydrogen atmosphere in our previous works have proved that hydrogen was firstly activated at Ru site, forming activated hydrogen species (H*), the H* species was transferred to the surface of NiO by spill-over effect of Ni sites, resulting in the reduction of some oxidized Ni atoms to some extent.[43] For RuNi/C-480–PVP, the clear lattice fringes with spacing of 0.255 nm is attributed to RuO_2 (101) (JCPDS card no. 43-1027) (Fig. 4c and d). With regard to RuNi/C-680–PVP, the typical core–thin shell structure characteristic can be seen in Fig. 4e, the RuNi NP in the white square. The HRTEM image for RuNi/C-680–PVP shows lattice fringes with an interplanar spacing of 0.234 nm in the core, corresponding to the Ru (100) planes (Fig. 4f). It suggests that RuO_2 could be reduced by carbon (Scheme 1) and was transferred inside the RuNi NPs at high temperature because of different surface energy of Ru and Ni (Ru = 3.043 J m^{-2}, however, Ni = 2.380 J m^{-2}).[70] It is very consistent with the XRD patterns and XPS spectra for RuNi/C-680–PVP.

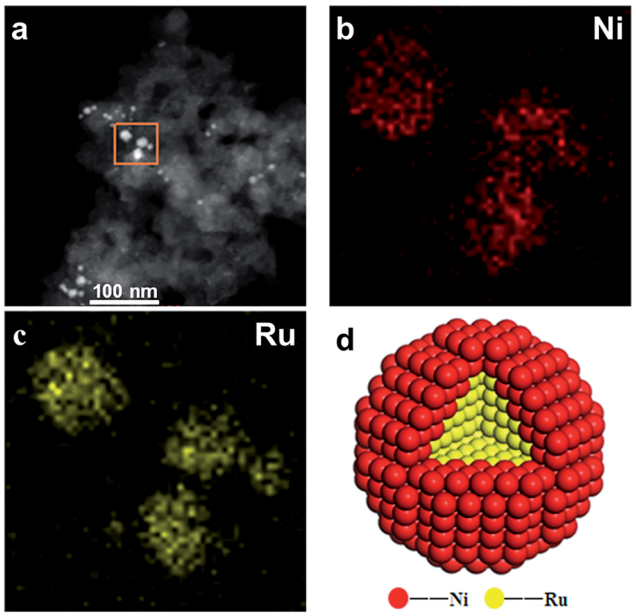

Fig. 5 (a) HAADF-STEM image, (b and c) EDS mapping of Ni (red) and Ru (yellow), and (d) the atomic model structure for RuNi NPs in the RuNi/C-680–PVP sample, respectively.

3.5 Elemental mapping and line-scanning measurement for the catalysts

To further obtain the RuNi nanostructure and elemental distributions in the RuNi/C-680–PVP catalyst, the elemental analysis was carried out by Cs-corrected high angle annular dark field-scanning transmission electron microscopy (HAADF-STEM) in combination with energy dispersive X-ray spectroscopy (EDS). Elemental mapping analysis for RuNi NPs in the RuNi/C-680–PVP sample (Fig. 5) demonstrates that the distribution range of Ni is slightly larger than that of Ru, clearly indicating the formation of Ru@Ni core–thin shell structure in this sample, with a good agreement with the XRD patterns, XPS spectra and HRTEM images for this sample. The model structure of Ru@Ni core–thin shell in RuNi/C-680–PVP is also vividly portrayed in Fig. 5d. Fig. 6 shows the line profiles for Ru and Ni element obtained by scanning e-beam across single RuNi BNP in RuNi/C-680–PVP. It can be clearly seen that the Ru peak

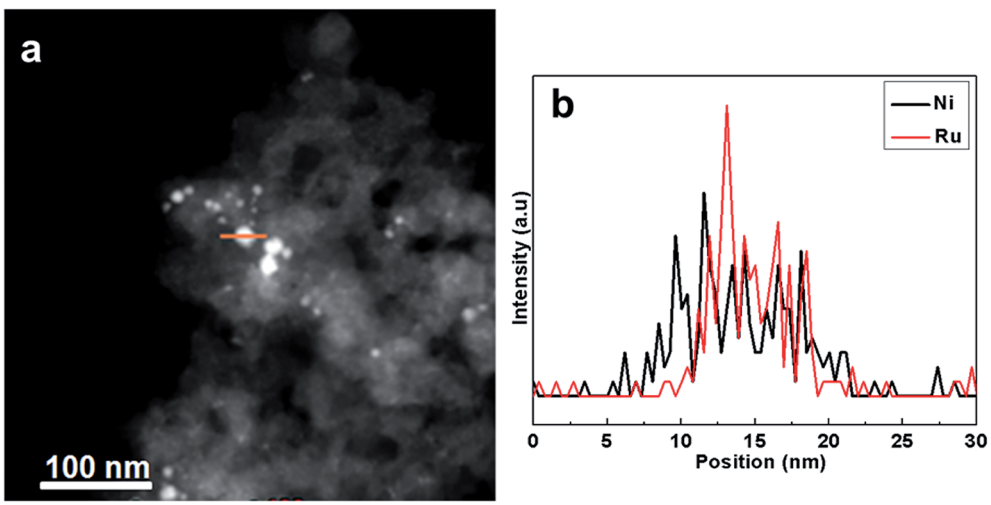

Fig. 6 (a) HAADF-STEM image for the RuNi/C-680–PVP sample. (b) The cross sectional compositional line-scanning profile for single RuNi NP in the RuNi/C-680–PVP sample.

(red line) is slightly narrower than the Ni peak (green line), further confirming Ru core coated with thin Ni shell, also indicating that Ni shell is very thin in this RuNi BNP.

3.6 HS-LEIS results of the catalysts

In order to obtain sufficient evidence to explain the formation of different RuNi nanostructures in the RuNi/C-380–PVP and RuNi/C-680–PVP samples, high-sensitivity low-energy ion scattering (HS-LEIS) measurements have been carried out. Fig. 7A demonstrates that Ru and Ni atoms co-exist on the outmost surface of RuNi/C-380–PVP, whereas the intensity of Ru signal is much stronger than that of Ni signal. Therefore, it can be further concluded that Ru atoms were mainly on the surface of RuNi NPs in the RuNi/C-380–PVP catalyst. The HS-LEIS spectra for the RuNi/C-680–PVP sample are displayed in Fig. 7B and C. Only Ni signal can be observed, indicating only Ni atoms on the outmost surface of RuNi NPs. To obtain the Ru and Ni composition of different atom layers of the catalysts, they were forcefully sputtered with a Ne^+ beam energy of 5 keV and a current of 5 nA for different lengths of time. With the sputtering time increasing from 120 s to 480 s, still only the Ni signal can be observed, without any Ru signal for RuNi/C-680–PVP (<600 s). But when the sputtering time increased to 720 s, the Ru atoms could be detected, implying that Ni shell was very thin. Therefore, the HS-LEIS results further provide evidence for the formation of Ru@Ni core–thin shell in the RuNi/C-680–PVP catalyst. The electron interaction between the Ni thin shell and Ru atoms on the surface of Ru core probably resulted in the catalytic activity of RuNi/C-680–PVP (actually in format of Ru@thin Ni/C) for the hydrogenation of benzene to cyclohexane much higher than that of the Ni/NiO/C and Ru/C catalysts. The mechanism of the improvement in the catalytic performance of the Ru@thin Ni/C catalyst will be further investigated in our follow-up works.

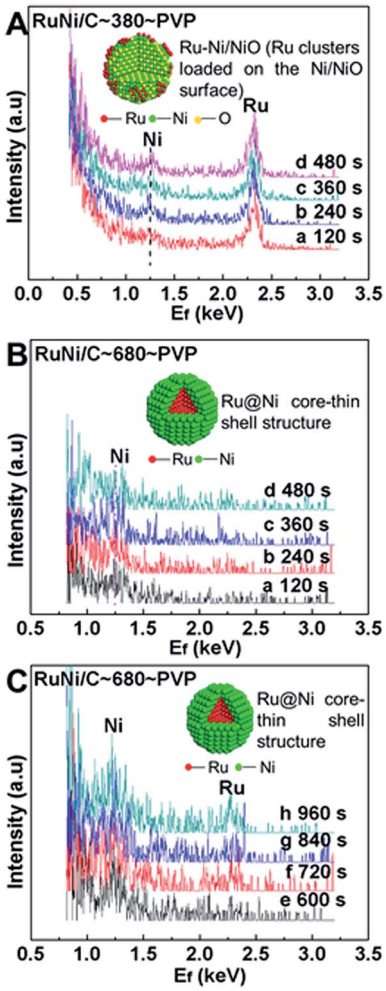

Fig. 7 (A) 5 keV $^{20}Ne^+$ HS-LEIS spectra for the RuNi/C-380–PVP sample after sputtered with a Ne^+ beam energy of 5 keV and a current of 5 nA for different lengths of time. (a) 120 s, (b) 240 s, (c) 360 s and (d) 480 s. (B and C) 5 keV $^{20}Ne^+$ HS-LEIS spectra for the RuNi/C-680–PVP sample after sputtered with a Ne^+ beam energy of 5 keV and a current of 5 nA for different lengths of time. (a) 120 s, (b) 240 s, (c) 360 s, (d) 480 s, (e) 600 s, (f) 720 s, (g) 840 s and (h) 960 s. E_f = energy of backscattered ion.

4. Conclusions

In summary, the Ru nanoclusters supported on Ni/NiO NPs, RuO_2 nanoparticles-on-NiO nanoparticles and Ru@Ni core–thin shell nanostructures were successfully prepared by varying the temperature of thermal treatment of RuNi/C-uncalcined–PVP in flowing N_2 and the characterizations have simultaneously proved these various nanostructures of RuNi NPs in the catalysts. Additionally, the chemical states of Ru and Ni, and RuNi NPs size were well controlled by adjusting the annealing temperature. This work indicated that the RuNi/C-380–PVP catalyst (Ru nanoclusters supported on Ni/NiO NPs) was 3–4 times more active than RuNi/C-680–PVP (Ru@Ni/C-core–thin shell) for benzene hydrogenation to cyclohexane, due to the synergetic effect of Ru (activating H_2), NiO (activating benzene) and Ni sites (as a "bridge" for transferring activated H species to the activated benzene). On the other hand, RuNi/C-480–PVP (RuO_2/NiO/C) showed no activity for this reaction because of existing RuO_2 which was unfavorable for activating hydrogen molecular. This work also provides a novel method to design and prepare the catalysts with specific nanostructure, to effectively exploit each noble and non-noble metal atom.

Acknowledgements

This work was supported by the Doctor Starting Foundation of Jiangxi University of Science and Technology of China (Grant No. jxxjbs15008), National Natural Science Foundation of China (Grant No. 201106118, 21303140, 21263005, 21206062 and 21466013), the Natural Science Foundation of Jiangxi Province of China (Grant No. 20143ACB21018), and the Landing Project of Science and Technology of Colleges and Universities in Jiangxi Province (KJLD14046).

Notes and references

1 V. Mazumder, M. Chi, M. N. Mankin, Y. Liu, O. N. Metin, D. Sun, K. L. More and S. Sun, *Nano Lett.*, 2012, **12**, 1102–1106.

2 N. S. Porter, H. Wu, Z. Quan and J. Fang, *Acc. Chem. Res.*, 2013, **46**, 1867–1877.
3 H. J. Kim, S. M. Choi, S. H. Nam, M. H. Seo and W. B. Kim, *Appl. Catal., A*, 2009, **352**, 145–151.
4 V. Petkov, Y. Ren, S. Shan, J. Luo and C.-J. Zhong, *Nanoscale*, 2014, **6**, 532–538.
5 X. Wei, X.-F. Yang, A.-Q. Wang, L. Li, X.-Y. Liu, T. Zhang, C.-Y. Mou and J. Li, *J. Phys. Chem. C*, 2012, **116**, 6222–6232.
6 S. Shan, V. Petkov, L. Yang, J. Luo, P. Joseph, D. Mayzel, B. Prasai, L. Wang, M. Engelhard and C.-J. Zhong, *J. Am. Chem. Soc.*, 2014, **136**, 7140–7151.
7 J. Pritchard, M. Piccinini, R. Tiruvalam, Q. He, N. Dimitratos, J. A. Lopez-Sanchez, D. J. Morgan, A. F. Carley, J. K. Edwards, C. J. Kielyb and G. J. Hutchings, *Catal. Sci. Technol.*, 2013, **3**, 308–317.
8 D. I. Enache, J. K. Edwards, P. Landon, B. Solsona-Espriu, A. F. Carley, A. A. Herzing, M. Watanabe, C. J. Kiely, D. W. Knight and G. J. Hutchings, *Science*, 2006, **311**, 362–365.
9 R. Loukrakpam, S. Shan, V. Petkov, L. Yang, J. Luo and C.-J. Zhong, *J. Phys. Chem. C*, 2013, **117**, 20715–20721.
10 L. Yang, S. Shan, R. Loukrakpam, V. Petkov, Y. Ren, B. N. Wanjala, M. H. Engelhard, J. Luo, J. Yin, Y. Chen and C.-J. Zhong, *J. Am. Chem. Soc.*, 2012, **134**, 15048–15060.
11 S. Shan, J. Luo, L. Yang and C.-J. Zhong, *Catal. Sci. Technol.*, 2014, **4**, 3570–3588.
12 L. Kesavan, R. Tiruvalam, M. H. Ab Rahim, M. I. bin Saiman, D. I. Enache, R. L. Jenkins, N. Dimitratos, J. A. Lopez-Sanchez, S. H. Taylor and D. W. Knight, *Science*, 2011, **331**, 195–199.
13 X. Huang, Y. Li, H. Zhou, X. Zhong, X. Duan and Y. Huang, *Chem.–Eur. J.*, 2012, **18**, 9505–9510.
14 D. Wang, H. L. Xin, R. Hovden, H. Wang, Y. Yu, D. A. Muller, F. J. DiSalvo and H. D. Abruña, *Nat. Mater.*, 2013, **12**, 81–87.
15 J. Luo, P. N. Njoki, Y. Lin, D. Mott, L. Wang and C.-J. Zhong, *Langmuir*, 2006, **22**, 2892–2898.
16 G. Chen, S. Desinan, R. Nechache, R. Rosei, F. Rosei and D. Ma, *Chem. Commun.*, 2011, **47**, 6308–6310.
17 K. C. Pingali, S. Deng and D. A. Rockstraw, *Powder Technol.*, 2008, **187**, 19–26.
18 N. Cao, J. Su, X. Hong, W. Luo and G. Cheng, *Chem.–Asian J.*, 2014, **9**, 562–571.
19 G. Chen, S. Desinan, R. Rosei, F. Rosei and D. Ma, *Chem.–Eur. J.*, 2012, **18**, 7925–7930.
20 J. Li, M. Qiao and J.-F. Deng, *J. Mol. Catal. A: Chem.*, 2001, **169**, 295–301.
21 H. Li and Y. Xu, *Mater. Lett.*, 2001, **51**, 101–107.
22 F. Domínguez, J. Sánchez, G. Arteaga and E. Choren, *J. Mol. Catal. A: Chem.*, 2005, **228**, 319–324.
23 L. J. Simon, J. G. van Ommen, A. Jentys and J. A. Lercher, *J. Catal.*, 2001, **201**, 60–69.
24 A.-G. A. Ali, L. I. Ali, S. M. Aboul-Fotouh and A. K. Aboul-Gheit, *Appl. Catal., A*, 1998, **170**, 285–296.
25 L. Simon, J. Van Ommen, A. Jentys and J. Lercher, *Catal. Today*, 2002, **73**, 105–112.
26 J. Wang, Q. Li and J. Yao, *Appl. Catal., A*, 1999, **184**, 181–188.
27 T. Jiang, L. Lu, X. Yang, Q. Zhao, T. Tao, H. Yin and K. Chen, *J. Porous Mater.*, 2008, **15**, 67–73.
28 C.-S. Chen, J.-H. Lin, H.-W. Chen and C.-Y. Wang, *Catal. Lett.*, 2005, **105**, 149–155.
29 G. Süss-Fink, B. Mollwitz, B. Therrien, M. Dadras, G. Laurenczy, A. Meister and G. Meister, *J. Cluster Sci.*, 2007, **18**, 87–95.
30 S. Niembro, S. Donnici, A. Shafir, A. Vallribera, M. L. Buil, M. A. Esteruelas and C. Larramona, *New J. Chem.*, 2013, **37**, 278–282.
31 A. Nowicki, Y. Zhang, B. Léger, J.-P. Rolland, H. Bricout, E. Monflier and A. Roucoux, *Chem. Commun.*, 2006, 296–298.
32 M. Takasaki, Y. Motoyama, K. Higashi, S. H. Yoon, I. Mochida and H. Nagashima, *Chem.–Asian J.*, 2007, **2**, 1524–1533.
33 S. Miao, Z. Liu, B. Han, J. Huang, Z. Sun, J. Zhang and T. Jiang, *Angew. Chem., Int. Ed.*, 2006, **45**, 266–269.
34 K. X. Yao, X. Liu, Z. Li, C. C. Li, H. C. Zeng and Y. Han, *ChemCatChem*, 2012, **4**, 1938–1942.
35 M. Zahmakıran, Y. Tonbul and S. Özkar, *J. Am. Chem. Soc.*, 2010, **132**, 6541–6549.
36 Y. Ma, Y. Huang, Y. Cheng, L. Wang and X. Li, *Appl. Catal., A*, 2014, **484**, 154–160.
37 T. Ioannides and X. E. Verykios, *J. Catal.*, 1993, **143**, 175–186.
38 B. Yoon, H.-B. Pan and C. M. Wai, *J. Phys. Chem. C*, 2009, **113**, 1520–1525.
39 A. Louloudi and N. Papayannakos, *Appl. Catal., A*, 1998, **175**, 21–31.
40 B. Pawelec, V. La Parola, R. M. Navarro, S. Murcia-Mascarós and J. L. G. Fierro, *Carbon*, 2006, **44**, 84–98.
41 H. Duan, D. Wang, Y. Kou and Y. Li, *Chem. Commun.*, 2013, **49**, 303–305.
42 A. M. Venezia, V. L. Parola, B. Pawelec and J. L. G. Fierro, *Appl. Catal., A*, 2004, **264**, 43–51.
43 L. Zhu, Y. Jiang, J. Zheng, N. Zhang, C. Yu, Y. Li, C.-W. Pao, J.-L. Chen, C. Jin, J.-F. Lee, C.-J. Zhong and B. H. Chen, *Small*, 2015, **11**, 4385–4393.
44 L. Zhu, M. Cao, L. Li, H. Sun, Y. Tang, N. Zhang, J. Zheng, H. Zhou, Y. Li, L. Yang, C.-J. Zhong and B. H. Chen, *ChemCatChem*, 2014, **6**, 2039–2046.
45 L. Zhu, L. Zheng, K. Du, H. Fu, Y. Li, G. You and B. H. Chen, *RSC Adv.*, 2013, **3**, 713–719.
46 C. Wang, X. Han, P. Xu, J. Wang, Y. Du, X. Wang, W. Qin and T. Zhang, *J. Phys. Chem. C*, 2010, **114**, 3196–3203.
47 Y. Li, L. Zhu, K. Yan, J. Zheng, B. H. Chen and W. Wang, *Chem. Eng. J.*, 2013, **226**, 166–170.
48 Y. Li, Q. Zhang, N. Zhang, L. Zhu, J. Zheng and B. H. Chen, *Int. J. Hydrogen Energy*, 2013, **38**, 13360–13367.
49 Y. Huang, Y. Ma, Y. Cheng, L. Wang and X. Li, *Ind. Eng. Chem. Res.*, 2014, **53**, 4604–4613.
50 Y. Huang, Y. Ma, Y. Cheng, L. Wang and X. Li, *Catal. Commun.*, 2015, **69**, 55–58.
51 J. Zhang, K. Sasaki, E. Sutter and R. R. Adzic, *Science*, 2007, **315**, 220–222.
52 H. Ohtani, R. J. Wilson, S. Chiang and C. M. Mate, *Phys. Rev. Lett.*, 1993, **60**, 180–183.

53 J. P. Rabe and S. Buchholz, *Phys. Rev. Lett.*, 1991, **66**, 2096–2099.
54 U. G. Hong, J. K. Kim, J. Lee, J. K. Lee, J. H. Song, J. Yi and I. K. Song, *Appl. Catal., A*, 2014, **469**, 466–471.
55 M. Endo, Y. A. Kim, T. Takeda, S. H. Hong, T. Matusita, T. Hayashi and M. S. Dresselhaus, *Carbon*, 2001, **39**, 2003–2010.
56 H.-B. Zhang, G.-D. Lin, Z.-H. Zhou, X. Dong and T. Chen, *Carbon*, 2002, **40**, 2429–2436.
57 Y. Wu, R. Balakrishna, M. V. Reddy, A. S. Nair, B. V. R. Chowdari and S. Ramakrishna, *J. Alloys Compd.*, 2012, **517**, 69–74.
58 K.-W. Park, J.-H. Choi, B.-K. Kwon, S.-A. Lee, Y.-E. Sung, H.-Y. Ha, S.-A. Hong, H. Kim and A. Wieckowski, *J. Phys. Chem. B*, 2002, **106**, 1869–1877.
59 Y. Goto, K. Taniguchi, T. Omata, S. Otsuka-Yao-Matsuo, N. Ohashi, S. Ueda, H. Yoshikawa, Y. Yamashita, H. Oohashi and K. Kobayashi, *Chem. Mater.*, 2008, **20**, 4156–4160.
60 S. Sarkar, A. K. Sinha, M. Pradhan, M. Basu, Y. Negishi and T. Pal, *J. Phys. Chem. C*, 2010, **115**, 1659–1673.
61 N. Chakroune, G. Viau, S. Ammar, L. Poul, D. Veautier, M. M. Chehimi, C. Mangeney, F. Villain and F. Fiévet, *Langmuir*, 2005, **21**, 6788–6796.
62 Y. Yamauchi, T. Ohsuna and K. Kuroda, *Chem. Mater.*, 2007, **19**, 1335–1342.
63 K. Lasch, L. Jörissen and J. Garche, *J. Power Sources*, 1999, **84**, 225–230.
64 J. Bandara, C. M. Divarathne and S. D. Nanayakkara, *Sol. Energy Mater. Sol. Cells*, 2004, **81**, 429–437.
65 L. Zhu, Z. Yang, J. Zheng, W. Hu, N. Zhang, Y. Li, C.-J. Zhong, H. Ye and B. H. Chen, *J. Mater. Chem. A*, 2015, **3**, 124–132.
66 L. Zhu, H. Sun, H. Fu, J. Zheng, N. Zhang, Y. Li and B. H. Chen, *Appl. Catal., A*, 2015, **25**, 124–132.
67 L. Zhu, H. Sun, Z. Cao, J. Zheng, N. Zhang and B. H. Chen, *CIESC J.*, 2015, **88**, 3091–3097.
68 W. C. Conner Jr and J. L. Falconer, *Chem. Rev.*, 1995, **95**, 759–788.
69 R. Prins, *Chem. Rev.*, 2012, **112**, 2714–2738.
70 L. Vitos, A. V. Ruban, H. L. Skriver and J. Kollár, *Surf. Sci.*, 1998, **411**, 186–202.